RESEARCH ARTICLE | OCTOBER 24 2014

A novel micro-Raman technique to detect and characterize 4H-SiC stacking faults

N. Piluso; M. Camarda; F. La Via

J. Appl. Phys. 116, 163506 (2014)
https://doi.org/10.1063/1.4899985

JOURNAL OF APPLIED PHYSICS **116**, 163506 (2014)

A novel micro-Raman technique to detect and characterize 4H-SiC stacking faults

N. Piluso,[a] M. Camarda, and F. La Via
IMM-CNR, stradale primo sole, 50, 95121 Catania, Italy

(Received 26 June 2014; accepted 14 October 2014; published online 24 October 2014)

A novel Micro-Raman technique was designed and used to detect extended defects in 4H-SiC homoepitaxy. The technique uses above band-gap high-power laser densities to induce a local increase of free carriers in undoped epitaxies ($n < 10^{16}$ at/cm^{-3}), creating an electronic plasma that couples with the longitudinal optical (LO) Raman mode. The Raman shift of the LO phonon-plasmon-coupled mode (LOPC) increases as the free carrier density increases. Crystallographic defects lead to scattering or recombination of the free carriers which results in a loss of coupling with the LOPC, and in a reduction of the Raman shift. Given that the LO phonon-plasmon coupling is obtained thanks to the free carriers generated by the high injection level induced by the laser, we named this technique induced-LOPC (i-LOPC). This technique allows the simultaneous determination of both the carrier lifetime and carrier mobility. Taking advantage of the modifications on the carrier lifetime induced by extended defects, we were able to determine the spatial morphology of stacking faults; the obtained morphologies were found to be in excellent agreement with those provided by standard photoluminescence techniques. The results show that the detection of defects via i-LOPC spectroscopy is totally independent from the stacking fault photoluminescence signals that cover a large energy range up to 0.7 eV, thus allowing for a single-scan simultaneous determination of any kind of stacking fault. Combining the i-LOPC method with the analysis of the transverse optical mode, the micro-Raman characterization can determine the most important properties of unintentionally doped film, including the stress status of the wafer, lattice impurities (point defects, polytype inclusions) and a detailed analysis of crystallographic defects, with a high spectral and spatial resolution. © *2014 AIP Publishing LLC*. [http://dx.doi.org/10.1063/1.4899985]

I. INTRODUCTION

A. 4H-SiC material

Over the last two decades, Silicon Carbide has attracted wide interest being an excellent material for high-power, high-temperature, and high frequency devices. Accordingly, many characterization methods have been optimized to obtain better and faster detection of defects. While most harmful defects (such as micropipes) have been almost completely eliminated from the epitaxies, other defects degrade and hamper the proper functioning of SiC devices. Crystallographic defects, such as stacking faults (SFs), are currently the major issues that prevent the high yield of devices grown on large wafers (6 in.). One of the main aims in the 4H-SiC research field is to eliminate them from the epitaxial layer. Many of these SFs are highly damaging for unipolar high power SiC devices[1] and bipolar power devices,[2,3] increasing the leakage current and altering the I-V relation, reducing the reliability of the devices.[4–6]

Currently, the photoluminescence technique (PL) is the most used method to detect and study the nucleation and propagation of 4H-SiC crystallographic defects, in particular, SFs that can be generated in the substrate[7,8] and at the interface with the substrate or in the epilayer during growth processes.[9–11] Stacking faults characterization is important because they are featureless and invisible on optical microscopy. Moreover, optical methods are strongly recommended because they avoid complex and time consuming sample preparation, being non-destructive techniques. UV-PL imaging has been widely used for detection and study of defects, e.g., luminescence imaging of dislocations bounding stacking faults.[12] Extended defects in SiC, including SFs, Basal Plane Dislocations (BPD), crystalline inclusions and micropipes have been revealed and studied by PL imaging techniques.[13–15] Furthermore, recent results[16] related to the emission along partial dislocations bounding recombination-induced stacking faults in 4H-SiC pin diodes, demonstrated that hyperspectral imaging of luminescence from extended defects could also be performed, providing the simultaneous collection of both spatial and spectral information.

SFs manifest themselves as an error of stacking along the [0001] crystal direction, acting as carrier recombination centers (quasi-quantum wells).[17–20] Their formation energy is relatively low,[7,21] so that their nucleation and expansion, during epilayer growth, is very likely. Furthermore, studies have proven that some SFs, in particular, the Single Shockley stacking fault (SSF), are able to enlarge during forward bias in bipolar devices[3] or under laser excitation during PL characterization,[22–26] which in turn leads to a change in the basic device characteristics, such as the junction potential or the forward on-resistance R_{ON}.[27] A detailed model describing a possible driving force on SF expansion and contraction is provided by Caldwell *et al.*[28] Also, some authors[29] have shown the effect of extended defects on carrier lifetime. Time-resolved

[a]nicolo.piluso@imm.cnr.it. Tel.: +39 095 5968322

cathodoluminescence measurements have shown that near the regions where extended defects (SFs, Triangular Surface Defects, 3C-SiC inclusions) are found, carrier lifetimes are strongly reduced.

B. A novel micro-Raman spectroscopy approach

Micro-Raman spectroscopy is a powerful technique based on the inelastic scattering of light (usually supplied by a laser) by solid-state material. A typical Raman spectrum allows a rapid analysis of the phonon modes which incorporate many properties of the semiconductor material. The high spatial and spectroscopic resolution of the micro-Raman technique makes it suitable for the analysis of defects in thin film. Currently, the Micro-Raman technique can be used as a complementary method to PL imaging for SiC characterization thanks to the simultaneous collection of information related to the material probed, e.g., strain status, polytype inclusion, doping concentration.

Some authors have reported the relationship between SFs and Raman scattering[30–32] in the cubic polytype (3C-SiC). An enlargement and a shift of the TO Raman mode is observed for highly defective epilayers (as indicated by Rohmfeld *et al.*[31] which shows an appreciable enlargement of the TO Raman mode for high stacking fault density, with an average distance between the SFs of 20 nm) and in regions with intense stress fields.[33,34] Given the higher quality of 4H-SiChomoepitaxial films (characterized by much lower defect densities and stress fields) the enlargement and shift of the TO Raman mode cannot be used. Micro-Raman technique has been used to study the properties of SiC[35] and to detect extended defects[36] in highly defective regions by using the variation of the TO Raman mode that depends on the stacking fault density. Moreover, the UV-Raman technique has been used to detect comet defects in 4H-SiC[37] by probing the intensities of the Raman modes, and to characterize ion-implanted SiC crystals,[38] demonstrating that, by using a deep UV laser as excitation wavelength, micro-Raman spectroscopy is a powerful tool for investigating surface structures and surface defects.

An alternative method that allows the detection of defects (in particular, SFs) can be considered by using the longitudinal optical (LO) Raman mode. The atomic displacements associated with the LO phonon mode generate a longitudinal electric field (due to the partially ionic nature of the lattice and the difference in electronegativity between Silicon and Carbon atoms) which interacts with the neighboring electrons. In the case of high free-carrier density such a longitudinal electric field results in an additional interaction between the LO phonons mode and the free carriers.[39] The mathematical model that describes such an interaction is widely used and described in the literature,[40–42] it determines the doping[43,44] and the electron mobility[45] of thin films. Micro-Raman analysis has also been used along with the Hall effect and transmission measurements to extract carrier density profiles from SiC wafers.[46] Moreover, as described by some authors,[47] at high optical excitation the formation of a dense electron-hole plasma has been observed in many semiconductors (GaAs, GaP). Furthermore, under an intense laser excitation, the LO phonon-plasmon coupling mode has been detected and studied in undoped GaP crystal.[48] In this context the excess carriers, induced by laser pumping, are characterized by a carrier lifetime and electrical mobility, appearing as a local increase of carrier concentration that can be easily measured by Raman tools. These electrical properties are perturbed by crystallographic defects so that a systematical study of the local (induced) carrier density variation can be used to detect crystallographic defects. Free carrier redistribution, resulting from SF formation in annealed 4H-SiC, has been observed by some authors.[49] Based on these considerations a new Raman methodology analysis, called induced-LOPC (i-LOPC), was designed. The injection of free carriers by a laser with a wavelength lower than the material band edge (HeCd at 325 nm, 4H-SiC band-gap at 388 nm) with different power densities was used to study the effect of a crystallographic defect, such as SF or point defects, on a local increase of the carrier density. The interaction between the electronic plasma and the lattice vibration, through inelastic scattering, is related to the plasmon damping constant $\gamma = e/(m^*\mu)$, and the plasmon frequency $\omega^2{}_p = 4\pi n e^2/\varepsilon_{inf} m^*$, where e is electron charge, m^* is the electron effective mass, μ is the carrier mobility, and ε_{inf} is the high frequency dielectric constant, see Refs. 41 and 42 for details.

From this set of equations it is possible to extract n and μ, i.e., determine the doping and carrier mobility of the film.

It is interesting to note that, in general, the *effective* electron-hole pair density (n) is controlled by the equilibrium conditions between carrier generation (G) and recombination processes (U), this equilibrium can be expressed by the following expression:

$$U = G = n - n_0/\tau, \tag{1}$$

where n is the *equilibrium* carrier concentration, n_0 is the initial carrier concentration, τ is the minority carrier lifetime and G is the injection of carriers due to the laser exposure

$$G = \Phi\alpha e^{\alpha x}, \tag{2}$$

where Φ is the flux applied by the laser, α is the absorption coefficient, and x is the distance within the epitaxy at which the carriers are generated. In the case of high doped epitaxies, low laser densities or low carrier lifetimes $G\tau \ll n_0$ so that $n - n_0 \sim 0$, and no carrier *generation* can be revealed ($n \approx n_0$ 10^{18}). In these conditions, the standard Raman LOPC determines the film doping (n_0). On the other hand, in the case of low-doped epitaxies ($n_0 < 10^{15}$) and for high carrier injections ($\Phi > 10^{17}$) a substantial carrier generation can be observed and from Eqs. (1) and (2) carrier lifetime can be extracted.

We systematically compared the PL signal and the phonon modes to determine the nature of the perturbation generated by the defects observed in Raman spectra: crystallographic and stress field effects (TO mode sensitive) or electronic effects (LO mode sensitive).

II. EXPERIMENTAL DETAIL

Micro-Raman and PL maps were collected using an HR800 integrated system by Horiba Jobin Yvon in a back-

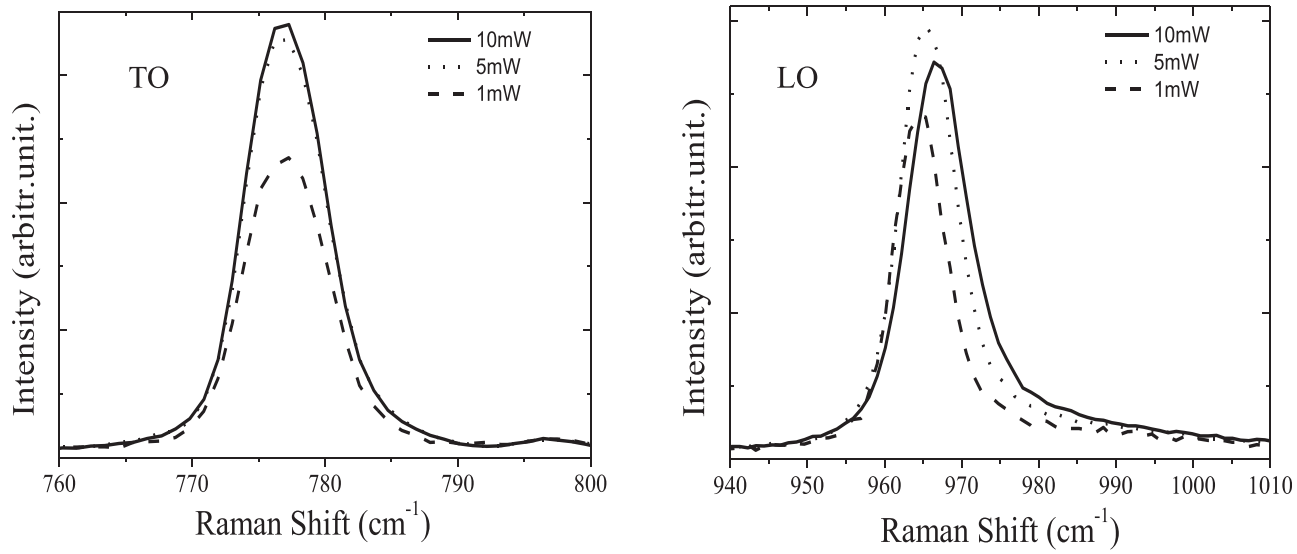

FIG. 1. TO (left) and LO (right) Raman modes acquired far from extended defects for different laser powers.

scattering configuration. The excitation source was supplied by an He-Cd laser with a wavelength of 325 nm and a variable, *on-sample,* power ranging from 1 to 10 mW (with a power density of about 0.5 to 5 kW/cm^2, respectively). The laser was focused via a ×40 objective onto the sample and then reflected onto a 2400 grooves/mm kinematic grating. At room temperature and under normal condition of temperature stability (±1 °C), the accuracy of the instrument is ±0.2 cm^{-1}. The spatial resolution achievable with the motorized stage is 0.5 μm, while the spot laser diameter is about 2 μm, i.e., about 80% of the laser intensity is contained in a 2 μm spot. In order to avoid a needless spatial overlap in the acquired maps, a spatial acquisition step of 3 μm or 4 μm was adopted. Each spectrum was collected with acquisition times less than 0.5 s.

4H-SiC homoepitaxial layers of different thickness (from 6 to 100 μm and with doping concentrations below the Raman limit sensitivity ($n < 10^{17}$ at/cm^{-3} (Ref. 46)) grown on 4° ⟨11–20⟩ off-axis Si-face substrates were analyzed. For comparison we also analyzed 4H-SiC substrates, which are characterized by high doping concentrations ($n \sim 10^{19}$ at/cm^{-3}), well within Raman sensitivity.

III. RESULTS AND DISCUSSION

The variation of the Raman spectrum, acquired far from defects, at different laser powers, was evaluated. The Raman modes (LO and TO) were acquired for a homoepitaxial 6 μm thick unintentionally doped ($n \sim 10^{14}$ at/cm^{-3}) 4H-SiC film, at different laser powers (from 1 to 10 mW). The excitation source was filtered to evaluate how the laser power affects the Raman modes. Figure 1 shows that TO is unchanged with laser power (except for the Raman peak intensity), with a peak value of 776.8 cm^{-1}, very close to the stress free value.[35,50] This is mainly due to the high quality of the material. Conversely, LO Raman mode underwent an evident shift towards high frequencies as laser power increased. This variation was due to an increase of electronic density (electron-hole pairs) correlated to the increased laser power. Through the analysis of the LOPC the free carrier concentration was calculated;[41,42,51] Table I shows the results.

The spectrum acquired at 1 mW showed the LO Raman mode centered at 965.1 cm^{-1} that represents the ideal position of an unintentionally doped 4H-SiC. For laser-power ≤1mW the supposed increase of carrier concentration was below the sensitivity of Raman tools. The spectrum acquired at 5 mW showed an evident increase of the Raman shift (965.7 cm^{-1}). The Raman shift increased further at 10 mW (967.1 cm^{-1}).

As stated above, this analysis was performed far from any crystallographic defect. In order to determine how SFs perturb the increase of free carriers, different spectra were acquired for different laser powers on SFs and compared with spectra acquired far from SFs. Figure 2 shows the comparison between Raman modes acquired on the defect and far from the defect for two laser powers. LO Raman mode did not change on or out of the SF when the laser-power was 1 mW being too low to appreciably increase the carrier density. Conversely, when 10 mW laser-power was used, the spectrum acquired on the SF showed a consistent reduction of Raman shift, suggesting a trapping of free carriers. Such an effect can be used to detect the presence of defects through Raman inspection. Figure 2 shows a reduction of Raman shift from 967.1 cm^{-1} (far from defect) to 965.4 cm^{-1} (on the defect). The latter value is very close to the ideal LO value of undoped4H-SiC, thus, an indicative value related to the effect of the SFs on carrier density reduction can be calculated. The carrier density corresponding to the LO Raman shift observed

TABLE I. LO Raman Shift, plasmon frequency and carrier density as a function of laser power.

Laser-power	Peak center (cm^{-1})	ω_p, plasmon frequency (cm^{-1})	n, carrier density (at/cm^{-3})
Laser at 1 mW	965.1	Not calculable	Not calculable
Laser at 5 mW	965.7	90	2×10^{17}
Laser at 10 mW	967.1	160	6.5×10^{17}

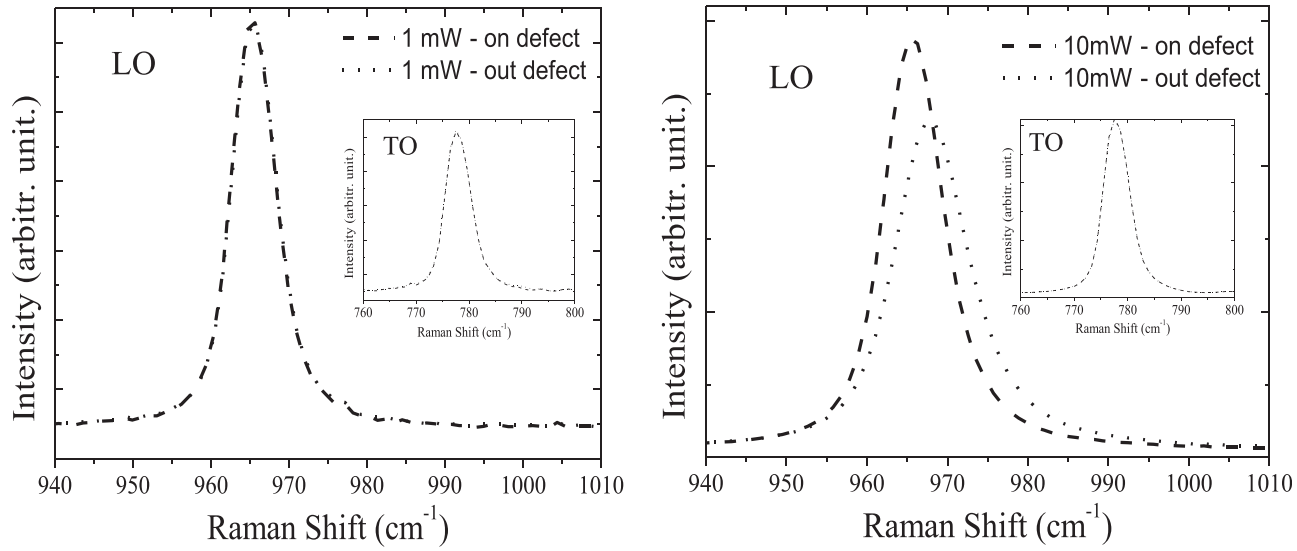

FIG. 2. LO Raman phonon mode acquired on and away from an extended defect for laser powers of 1 mW (left) and 10 mW (right). TO Raman mode is unchanged (inset).

under laser pumping at 10 mW was $\sim 6.5 \times 10^{17}$at/cm^{-3}. This represents the value of carrier density reduction under the action of an isolated SF. Although the extended defect determined a strong reduction of the free carrier concentration, a slight Raman shift of 0.3 cm^{-1} was noted between the spectra acquired on the defect when a high laser power was applied and far from defect when a low laser power was applied. It indicates that a very small coupling between LO Raman mode and free carrier remains on the defect. This is mainly due to two reasons: (1) the penetration depth of the laser is very high (7.5 μm,[52]) compared to the width of the SF that crosses the epitaxy as a tilted plane with respect to the growth axis, so that the free carriers are also generated above and below it; (2) the SF can trap a limited amount of free carriers that, probably, did not exceed a density of 6.5×10^{17}at/cm^{-3}. Figure 3 shows the detection of a particular SF by using PL and i-LOPC techniques. The spatial morphology and the PL spectrum determine the crystal structure of the defect. In particular, the triangular shape together with a PL signal centered at 2.7 eV are related to 4SSF, which is associated to a (4,4) stacking sequence in Zhdanov's notation.[20,53] The width of the defect along the[11–20] direction indicates that it was formed close to the epilayer-substrate interface (see Figure 3(A)).

Map (B) in Figure 3 was obtained from the analysis of the LO Raman mode shift performed across the same region characterized by the PL method. An evident modulation of the Raman shift can be observed. It detected the presence of

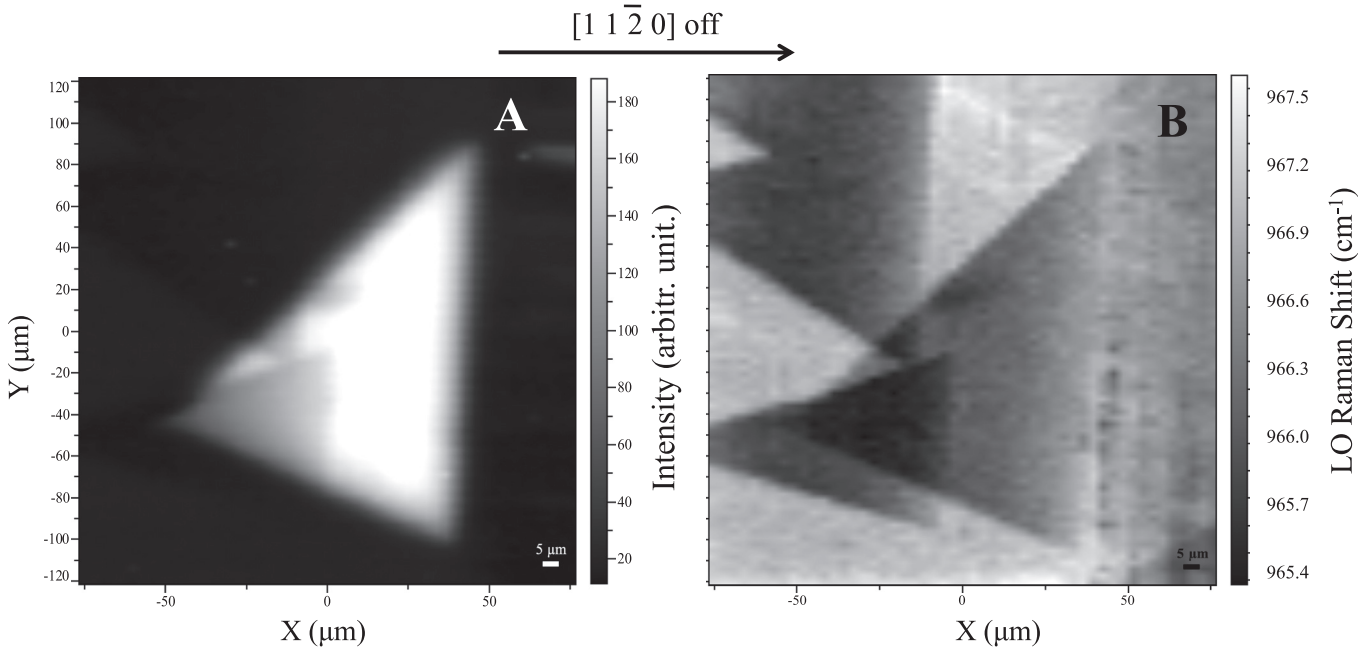

FIG. 3. (A) Stacking Fault (4SSF) observed at 2.7 eV by PL technique. (B) Stacking Fault (4SSF) observed at 965 cm^{-1} by Raman technique. Additional defects are noticed.

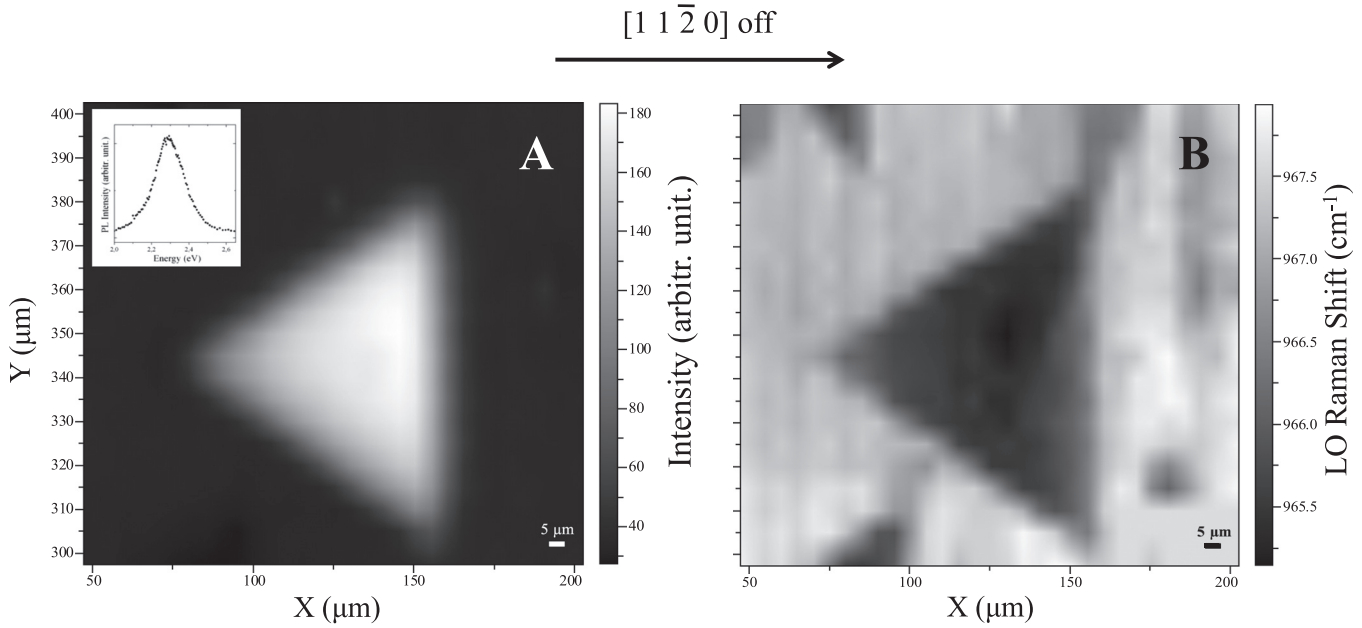

FIG. 4. (A) Defect with stacking sequence (10,2) in Zhadonov's notation, observed at 2.3 eV (as shown in the inset) by PL technique. (B) The same defect observed at 965 cm^{-1} by Raman technique.

a 4SSF, obtaining the same results achieved by the PL map (Fig. 3(A)). The modulation of the LO shift accurately reproduced the expected triangular shape. An additional LO Raman shift was observed around the 4SSF. Such a variation was related to another SF with different energy characteristics (PL peak) and thus not clearly seen through the PL technique (they can just be seen in Fig. 3(A) as darker areas). The high spectral resolution used allows a careful inspection of the Raman data, with a wavenumber range of about 1000 cm^{-1}, while it penalizes the PL analysis, as the energy range is about 0.1 eV.

Several SFs were detected and studied with this technique. Figure 4 shows an uncommon SF detected on a highly defective homoepitaxy. The SF appears triangular in shape with a photoluminescence signal located at 2.3 eV (as indicated by the inset in Figure 4(A)). Such an SF is expected to be a 4SSF with a stacking sequence of (10,2) in Zhadonov's notation.[20] Once again, the micro-Raman technique provided a detailed morphological map, indicating the presence of additional defective regions around the detected SF, which could not be directly seen by PL analysis in the spectral range shown.

Since the penetration depth (∼10 μm) was larger than the film thickness (∼6 μm), characterizations were performed on thicker samples (100 μm) and on substrates in order to decouple the effects of the latter from those of epitaxial films. Figure 5 shows an agglomeration of extended defects, principally hosting a Bar Shaped SF (BSSF) coming

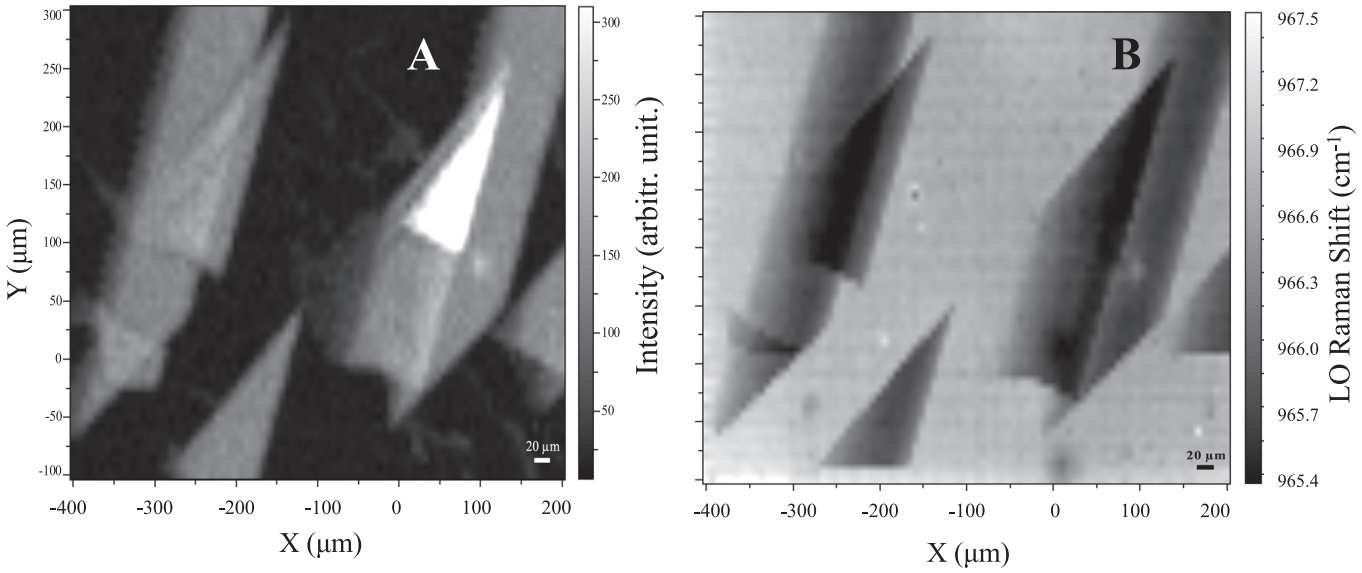

FIG. 5. (A) Stacking Faults observed at 2.93 eV by PL technique. (B) Stacking Faults observed at 965 cm^{-1} by Raman technique. Sample thickness 100 μm.

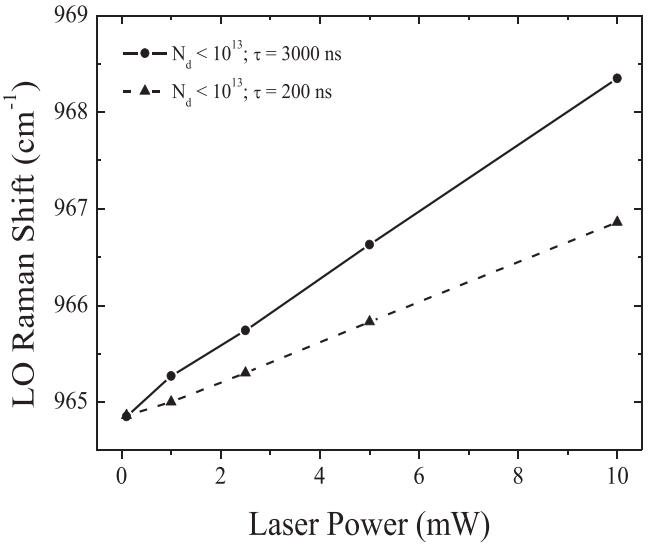

FIG. 6. LO Raman mode shift as a function of Laser Power.

from the defective substrate.[7] As shown by maps A and B of Figure 5, both techniques reproduced the complex morphology of the defects in the inspected region. On the other hand, analysis conducted on highly doped substrates, as expected, did not reproduce the above mentioned results (data not shown). The main reason being that the high doping concentration ($n \sim 10^{19}$ at/cm^{-3}), the electronic density reduction, produced by SFs (quantified in the order of 6.5×10^{17}at/cm^{-3}), was undetectable.

A subsequent analysis was conducted to determine the correlation between the LO Raman shift associated to the laser power, and the carrier lifetime (τ). Indeed, point defects such as interstitial and substitutional vacancies, depending on the location of the defect level within the band-gap, can act as scattering or recombination centers, reducing the average mobility or lifetime of the epitaxy.[45]

To verify such an assumption, two samples, with very thick homoepitaxy (100 μm) and large difference in carrier lifetime, were analyzed. The carrier lifetimes of the two samples (~200 ns and ~3 μs) were measured using the microwave-PCD technique.[54,55] The sample with the highest carrier lifetime underwent an oxidation process, which is known to reduce the density of deep-level point defects.[56,57] The trend of the LO Raman shift as a function of the laser power is reported in Figure 6. The highest value of LO Raman shift was observed for the oxidized sample. An evident conclusion is that the lowering of point defect density increases the electronic free path, determining a longer carrier lifetime than the "as grown" sample. We used the LOPC model[41,42] together with Eqs. (1) and (2) to determine the carrier lifetime (τ) and induce carrier density (n) in different samples. The results are shown in Figure 7 and demonstrate the strong reliability of the Raman method.

These results suggest that an electrical characterization (carrier lifetime, doping and mobility) of 4H-SiC epitaxial films could be carried out through micro-Raman spectroscopy by using the i-LOPC method.

The overall defect characterization, applicable to both extended and point defects, makes the Raman technique a very powerful non-destructive method to determine the general status of epitaxy, which could be further, extended to a quick large-wafer analysis.

IV. CONCLUSIONS

A novel Micro-Raman approach, based on the induction of Longitudinal optical phonon-plasmon coupling (i-LOPC), was used to detect extended defects in 4H-SiChomoepitaxy. The correlation between the laser-power and the LO Raman mode shift was observed and used to detect and study extended defects. For high laser-powers (>5 mW) the free carriers, generated by the, above band-gap excitation, tended to create an electronic plasma that coupled with the LO phonon mode (LOPC). The greater the laser-power the greater was the Raman shift of the LOPC. Such an effect was altered/reduced when a defect was detected. The LOPC

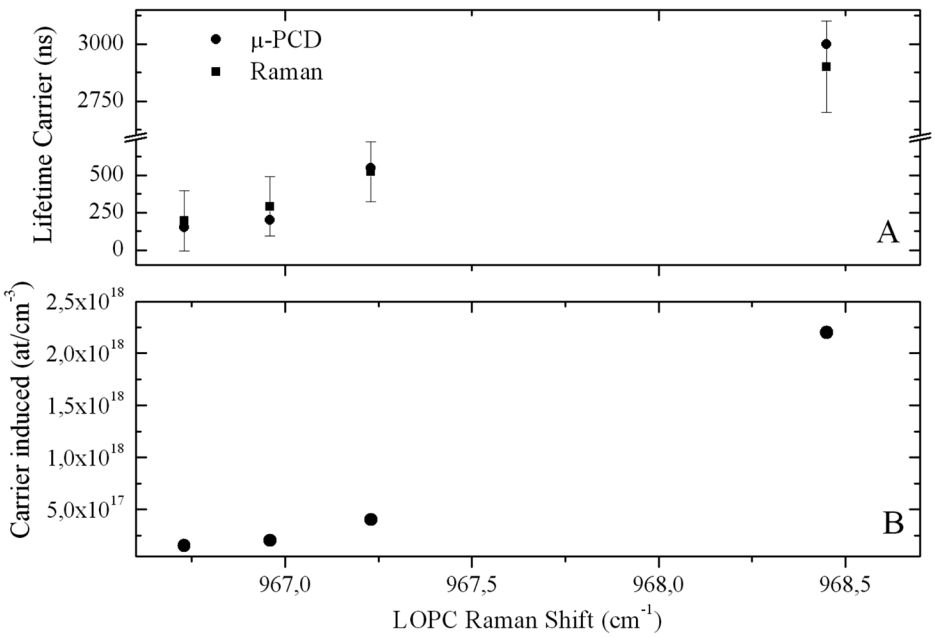

FIG. 7. (A) Comparison between the evaluation of carrier lifetime (τ) through μ-PCD and i-LOPC techniques. (B) Evaluation of carrier induced (n) by laser pumping.

mode shift was reduced on the defect because the free carriers underwent a redistribution over the defect,[49] emptying the free electron plasma. Thus, due to the defect, the LO phonon lost its plasmonic coupling, showing a Raman phonon mode that is typical for undoped 4H-SiC. This trapping mechanism is independent of the SF type thus allowing simultaneous identification of all SFs in the probed samples by acquiring a single Raman map. The results were compared with PL characterizations showing excellent agreement.

It should be mentioned that i-LOPC allows the identification of extended defects which do not generate intra-band-gap levels, such as (1,1,1,1) or (1,2,3) SFs,[19] which cannot be observed by PL analysis.

Finally, the i-LOPC method showed the connection between the carrier concentration induced by laser pumping and the carrier lifetime for undoped film, obtaining meaningful information related to the electrical properties of the film, and demonstrating that this technique is a fast, reliable and powerful method to characterize most crystallographic defects (extended and point defects) in the semiconductor field. Carrier lifetimes, deduced by the i-LOPC technique, were in very good agreement with the results obtained by the μ-PCD technique (see Fig. 7(A)).

Studies are underway to apply the i-LOPC method to other materials such as GaN and AlGaN.

ACKNOWLEDGMENTS

The authors would like to thank Dr. Marco Mauceri from E.T.C (Epitaxial Technology Center) for his contribution to this project.

[1]H. Lendenmann, F. Dahlquist, J. P. Bergman, H. Bleichner, and C. Hallin, Mater. Sci. Forum **389–393**, 1259 (2002).
[2]M. Skowronski and S. Ha, J. Appl. Phys. **99**, 011101 (2006).
[3]J. P. Bergman and H. P. A. U. P. Skytt, Mater. Sci. Forum **353–356**, 299 (2001).
[4]K. Nakayama, A. Tanaka, K. Asano, T. Miyazawa, and H. Tsuchida, Mater. Sci. Forum **740–742**, 903 (2013).
[5]A. Tanaka, K. Nakayama, K. Asano, T. Miyazawa, and H. Tsuchida, Jpn. J. Appl. Phys., Part 1 **52**, 04CP10-1 (2013).
[6]B. Chen, J. Chen, T. Sekiguchi, T. Ohyanagi, H. Matsuhata, A. Kinoshita, and H. Okumura, J. Electron. Mater. **39**, 684 (2010).
[7]M. Camarda, A. Canino, A. La Magna, F. La Via, G. Feng, T. Kimoto, M. Aoki, and H. Kawanowa, Appl. Phys. Lett. **98**, 051915 (2011).
[8]G. Feng, J. Suda, and T. Kimoto, Appl. Phys. Lett. **92**, 221906 (2008).
[9]G. Feng, J. Suda, and T. Kimoto, Phys. B **404**, 4745 (2009).
[10]G. Feng, J. Suda, and T. Kimoto, J. Electron. Mater. **39**, 1166 (2010).
[11]G. Feng, J. Suda, and T. Kimoto, Mater. Sci. Forum **615–617**, 245 (2009).
[12]K. X. Liu, R. E. stahlbush, S. L. Maximenko, and J. D. Caldwell, Appl. Phys. Lett. **90**, 153503 (2007).
[13]A. Galeckas, A. Hallen, S. Majdi, J. Linnros, and P. Pirouz, Phys. Rev. B **74**, 233203 (2006).
[14]R. E. Stahlbush, K. X. Liu, Q. Zhang, and J. J. Sumakeris, Mater. Sci. Forum **556–557**, 295 (2007).
[15]K. X. Liu, R. E. Stahlbush, M. E. Twigg, J. D. Caldwell, E. R. Glaser, K. D. Hobart, and F. J. Kub, J. Electron. Mater. **36**, 297 (2007).
[16]J. D. Caldwell, A. Giles, D. Lepage, D. Carrier, K. Moumanis, B. A. Hull, R. E. stahlbush, R. L. Myers-Ward, J. J. Dubowski, and M. Verhaegen, Appl. Phys. Lett. **102**, 242109 (2013).
[17]U. Lindefelt, H. Iwata, S. Oberg, and P. R. Briddon, Phys. Rev. B **67**, 155204 (2003).
[18]M. S. Miao, S. Limpijumnong, and W. Lambrecht, Appl. Phys. Lett. **79**, 4360 (2001).
[19]M. Camarda, P. Delugas, A. Canino, A. Severino, N. Piluso, A. La Magna, and F. La Via, Mater. Sci. Forum **645–648**, 283 (2010).
[20]M. Camarda, A. La Magna, P. Delugas, and F. La Via, Appl. Phys. Express **4**, 25802 (2011).
[21]W. J. Choyke, H. Matsunami, and G. Pens, *Silicon Carbide: Recent Major Advances* (Springer, Berlin, 2005), p. 89.
[22]A. Canino, M. Camarda, A. La Magna, and F. La Via, Mater. Res. Soc. **1246**, 59 (2010).
[23]T. Miyanagi, H. Tsuchida, I. Kamata, T. Nakamura, and K. Nakayama, Appl. Phys. Lett. **89**, 062104 (2006).
[24]N. Hoshino, M. Tajima, M. Naitoh, E. Okuno, and S. Onda, Mater. Sci. Forum **600–603**, 349 (2009).
[25]T. Fujimoto, T. Aigo, M. Nakabayashi, S. Sato, M. Katsuno, H. Tsuge, H. Yashiro, H. Hirano, T. Hoshino, and W. Ohashi, Mater. Sci. Forum **645–648**, 319 (2010).
[26]A. Canino, M. Camarda, and F. La Via, Mater. Sci. Forum **679–680**, 67 (2011).
[27]I. Deretzis, M. Camarda, F. La Via, and A. La Magna, Phys. Rev. B **85**, 235310 (2012).
[28]J. D. Caldwell, R. E. Stahlbush, M. G. Ancona, O. J. Glembocki, and K. D. Hobart, J. Appl. Phys. **108**, 044503 (2010).
[29]S. I. Maximenko, J. A. Freitas, Jr., P. B. Klein, A. Shrivastava, and T. S. Sudarshan, Appl. Phys. Lett. **94**, 092101 (2009).
[30]S. Nakashima, Y. Nakatake, Y. Ishida, T. Takahashi, and H. Okumura, Physica B **308**, 684 (2001).
[31]S. Rohmfeld, M. Hundhausen, and L. Ley, Phys. Status Solidi B **215**, 115 (1999).
[32]T. Mitani, S. Nakashima, H. Okumura, and H. Nakasawa, Mater. Sci. Forum **527–529**, 343 (2006).
[33]N. Piluso, R. Anzalone, M. Camarda, A. Severino, A. La Magna, G. D'Arrigo, and F. La Via, J. Raman Spectrosc. **44**, 299 (2013).
[34]N. Piluso, R. Anzalone, M. Camarda, A. Severino, A. La Magna, G. D'Arrigo, and F. La Via, Mater. Sci. Forum **679–680**, 141 (2011).
[35]S. Nakashima and H. Harima, Phys. Status Solidi A **162**, 39 (1997).
[36]S. Nakashima, Y. Nakatake, H. Harima, M. Katsuno, and N. Ohtani, Appl. Phys. Lett. **77**, 3612 (2000).
[37]T. Tomita, S. Matsuo, T. Okada, T. Kimoto, H. matsunami, T. Mitani, and S. Nakashima, Appl. Phys. Lett. **87**, 241906 (2005).
[38]S. Nakashima, T. Mitani, J. Senzaki, H. Okumura, and T. Yamamoto, J. Appl. Phys. **97**, 123507 (2005).
[39]P. Y. Yu and M. Cardona, *Fundamentals of Semiconductors*, 2nd ed. (Springer-Verlag Berlin Heidelberg, New York, 2003).
[40]G. Irmer, V. V. Toporov, B. H. Bairamov, and J. Monecke, Phys. Status Solidi B **119**, 595 (1983).
[41]H. Harima, S. Nakashima, and T. Uemura, J. Appl. Phys. **78**, 1996 (1995).
[42]M. Chafai, A. Jaouhari, A. Torres, R. Anton, E. Martin, J. Jimenez, and W. C. Mitchel, J. Appl. Phys. **90**, 5211 (2001).
[43]N. Piluso, A. Severino, M. Camarda, R. Anzalone, A. Canino, G. Condorelli, G. Abbondanza, and F. La Via, Mater. Sci. Forum **645–648**, 255 (2010).
[44]H. Yugami, S. Nakashima, A. Mitsuishi, A. Uemoto, M. Shigeta, K. Furukawa, A. Suzuki, and S. Nakajima, J. Appl. Phys. **61**, 354 (1987).
[45]N. Piluso, A. Severino, M. Camarda, A. Canino, A. La Magna, and F. La Via, Appl. Phys. Lett. **97**, 142103 (2010).
[46]J. D. Caldwell, O. J. Glembocki, S. M. Prokes, E. R. Glaser, K. D. Hobart, D. M. Hansen, G. Chung, A. V. Bolotnikov, and T. S. Sudarshan, J. Appl. Phys. **101**, 093506 (2007).
[47]H. Nather and L. G. Quagliano, J. Lumin. **30**, 50 (1985).
[48]H. Yugami, S. Nakashima, Y. Oka, M. Hangyo, and A. Mitsuishi, J. Appl. Phys. **60**, 3303 (1986).
[49]O. J. Glembocki, M. Skowronski, S. M. Prokes, D. K. Gaskill, and J. D. Caldwell, Mater. Sci. Forum **527–529**, 347 (2006).
[50]Z. C. Feng, A. J. Mascarenhas, W. J. Choyke, and J. A. Powell, J. Appl. Phys. **64**, 3176 (1988).
[51]J. C. Burton, L. Sun, M. Pophristic, S. J. Lakacs, F. H. Long, Z. C. Feng, and I. T. Ferguson, J. Appl. Phys. **84**, 6268 (1998).
[52]S. G. Sridhara, T. J. Eperjesi, R. P. Devaty, and W. J. Choyke, Mater. Sci. Eng. B **61–62**, 229 (1999).
[53]H. Fujiwara, T. Kimoto, T. Tojo, and H. Matsunami, Appl. Phys. Lett. **87**, 051912 (2005).
[54]M. Ichimura, H. Tajiri, Y. Morita, N. Yamada, and A. Usami, Appl. Phys. Lett. **70**, 1745 (1997).
[55]G. Chung, M. J. Loboda, M. F. MacMillan, J. Wan, and D. M. Hansen, Mater. Sci. Forum **556–557**, 323 (2007).
[56]T. Hiyoshi and T. Kimoto, Appl. Phys. Express **2**, 041101 (2009).
[57]T. Miyazawa and H. Tsuchida, J. Appl. Phys. **113**, 083714 (2013).